Proceedings of the Fourteenth (2020) ISOPE Pacific-Asia Offshore Mechanics Symposium **www.isope.org**
Dalian, China, November 22-25, 2020

ISBN 978-1-880653-83-8; ISSN 1946-004X

CFD Study of Free Surface Effect on Flow around a Surface-Piercing Cylinder

*Songtao Chen, Weiwen Zhao, Decheng Wan**

Computational Marine Hydrodynamics Lab (CMHL), State Key Laboratory of Ocean Engineering,
School of Naval Architecture, Ocean and Civil Engineering, Shanghai Jiao Tong University, Shanghai, China
*Corresponding author

ABSTRACT

With the widely application of cylinders in offshore structures, flow around cylinder has been investigated extensively to explore the mechanism behind it. Nevertheless, most experiments and numerical simulations focused on the single-phase flow and the two-phase flow around the surface-piercing cylinder which considers the existence of free surface has not received much attention. In the present work, free surface effect on the flow around a surface-piercing cylinder at the Re=27000 and Fr=0.8 is investigated. All the numerical simulations are conducted by the in-house CFD solver naoe-FOAM-SJTU, which is developed based on the open-source toolbox OpenFOAM. RANS equations with turbulence model are adopted to simulate the flow and VOF method is used to capture the free surface. The comparison with experiment and LES results by others shows that the current method is reliable and can capture the time-averaged characteristics. Through the analysis, it is found that the existence of free surface has a significant influence on the hydrodynamic forces and the wake flow characteristics. A reduction of drag coefficient can be observed. The delayed transition of the shear layers and the attenuation of regular vortex shedding can be found near the free surface.

KEY WORDS: CFD; free surface; surface-piercing cylinder; RANS; VOF

INTRODUCTION

With the rapid development of offshore platforms such as spars and semi-submersibles, it is necessary to study the flow characteristics of them. So as the basic hydrodynamic problem, the flow around cylinder has received much attention because it can reveal complex flow phenomenon like separation, reattachment and vortex shedding. And with the help of computational fluid dynamics (CFD), we can get more detailed information including streamlines, velocity profiles and vortical structures to explore the mechanism behind it.

However, most experiments and numerical simulations (Williamson, 2003; Yeon et al., 2016; Pereira et al., 2019; Ye et al., 2017; Zhao et al., 2016) are about single-phase flow around the cylinder which ignores the effect of free surface. Actually, the existence of free surface makes the flow more complicated due to the interaction between air and water. Bow wave at the front, depression behind the cylinder and Kelvin wave in the far field can be observed. So, it is of great importance to study the effect of free surface for future work.

There are some studies investigating the flow around the surface-piercing cylinder. Inoue et al. (1993) experimentally investigated the flow around the vertical surface piercing cylinder on two cases which are Re=27000 and Fr=0.8 and Re=29000 and Fr=1.0 respectively. Chaplin et al. (2003) conducted a series of towing tank experiments of surface-piercing cylinder at a constant ratio (Re/Fr) of 2.79×10^9 . As for numerical simulations, Kawamura et al. (2002) used large eddy simulation (LES) to study the influence of Froude number varying from 0.2 to 0.8 about the flow around the surface-piercing cylinder. Yu et al. (2008) used LES and VOF (volume of fluid) method to study the flow structures and the loadings at various Reynolds numbers and Froude numbers. Suh et al. (2011) studied the vortical structures from the perspective of Reynolds stresses using a Lagrangian dynamic subgrid-scale model and the level set method. Koo (2011) used a coupled level set and VOF method (CLSVOF) to study the effect of Reynolds numbers and Froude numbers especially for the air-water interface structures.

The main objective of the present work is to study the effect of free surface on flow around a surface piercing cylinder using the CFD approach. In this paper, RANS equations with VOF method are adopted to simulate the flow. The brief introduction about the numerical method is presented in section 2. And details of the simulation setup are described in section 3. In section 4, the results obtained are compared with the experiment and LES simulations by others. And the conclusions of the free surface effect are got through the analysis.

NUMERICAL METHOD

Our in-house CFD solver naoe-FOAM-SJTU, which is developed on the open-source toolbox OpenFOAM, is used for all simulations. The reliability and accuracy of it have been proved in many complex viscous flow problems in marine hydrodynamics including the ship resistance test, ship propeller-rudder interaction, ship breaking bow waves and so

on (Wang et al., 2019). The free surface, which is an essential part in two-phase flow, is captured by the VOF (volume of fluid) method.

Governing equations

In current simulations, the flow is described by the incompressible Reynolds-Averaged Navier-Stokes (RANS) equations including the continuity equation. The governing equations are given as follows:

$$\nabla \cdot U = 0 \tag{1}$$

$$\frac{\partial \rho U}{\partial t} + \nabla \cdot (\rho U U) = -\nabla p_d - g \cdot x \nabla \rho + \nabla \cdot (\mu_{eff} \nabla U) + (\nabla U) \cdot \nabla \mu_{eff} + f_\sigma + f_s \tag{2}$$

Here, U is the velocity, $p_d = p - \rho g \cdot x$ denotes the dynamic pressure which is obtained by subtracting static pressure from the total pressure. ρ is the mixed density of air and water and g is the gravitational acceleration. $\mu_{eff} = \rho(\nu + \nu_t)$ represents the effective dynamic viscosity, where ν and ν_t are kinematic viscosity and eddy viscosity respectively. f_σ is a surface tension term and f_s is a source term which is added for the sponge layer.

The *SST* k-ω turbulence model is adopted to close the RANS equations by modelling the Reynolds stress. This turbulence model combines the k-ε and k-ω models so as to synthesize their respective advantages. The former is suitable for flow away from the walls while the latter is capable of predicting the boundary flow near the wall under adverse pressure gradients. The accuracy of this turbulence model has been validated for the similar cases and it is recommended to solve such problems which involves the adverse pressure gradients and flow separation (Zhang, 2017).

VOF method

The VOF (volume of fluid) method with artificial compression technique is applied to capture the interface in our simulations. And the transport equation is given as follows:

$$\frac{\partial \alpha}{\partial t} + \nabla \cdot (\alpha U) + \nabla \cdot (\alpha(1-\alpha) U_r) = 0 \tag{3}$$

where α represents the volume fraction in each cell. According to the value of α, it can be expressed as follows:

$$\begin{cases} \alpha = 0 & \text{air} \\ 0 < \alpha < 1 & \text{interface} \\ \alpha = 1 & \text{water} \end{cases} \tag{4}$$

The third term in Eq. 3 is an artificial compression term to ensure the sharpness of the interface and thereby reduce the smearing. U_r is the modeled velocity to compress the interface and it is normal to the interface. The description of U_r is given by:

$$U_r = \min\left\{ C_\alpha \frac{|\phi|}{|S_f|}, \max\left[\frac{|\phi|}{|S_f|} \right] \right\} n_f \tag{5}$$

where ϕ is the face volume flux, S_f is the cell face area vector, n_f is the face centered interface normal vector and C_α is a user specified parameter indicating the degree of compression. Here, C_α is set as 1 as default.

SIMULATION SETUP

Computational Domain and Mesh

The size of the computational domain is 40D×30D×6D (length×width×depth). The immersed length of the cylinder is 4D, with D the diameter of the cylinder. And the cylinder is placed in the center of the domain to minimize the impact of the boundary. Besides, the sponge layers are set up near the sides and outlet to absorb the reflected waves. Fig. 1 shows the sketch and main parameters of the computational domain.

As shown in Fig. 2, the unstructured mesh generated by snappyHexMesh is used for present simulations. In order to capture the free surface and the wake flow characteristics, the local mesh is refined in the vicinity of the interface and the geometry. In addition, 8 prism cell layers are fitted on the cylinder surface to make the non-dimensional distance y+<1 during the simulation, as shown in Fig. 2(c). The height of the first-layer cell is set as 0.002D. Three sets of mesh named Coarse (3.4M), Medium (5.8M) and Fine (7.9M) are adopted to study the influence of mesh density. The background mesh size in region I are 1/3D, 2/7D and 1/4D respectively, as shown in Fig.2(a). The finest mesh size (not include the prism cell layers) in region II are 1/12D, 1/14D and 1/16D respectively.

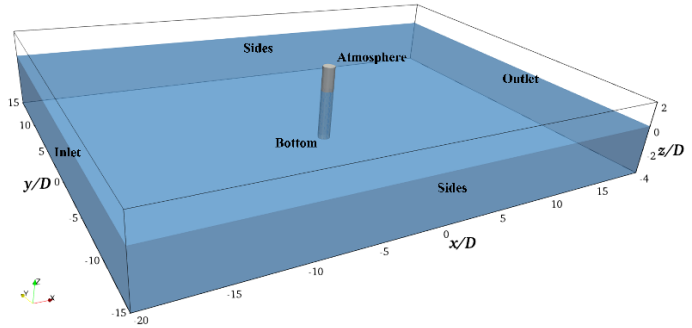

Fig 1. Computational domain

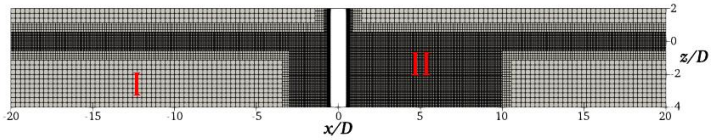

(a)Slice of the mesh at y=0 plane

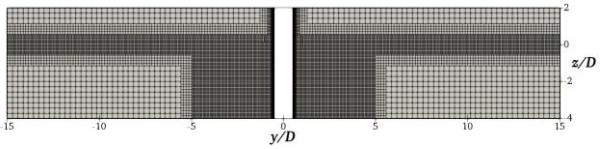

(b) Slice of the mesh at x=0 plane

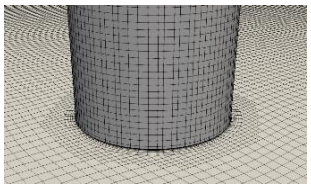

(c) Refined local mesh
Fig 2. Computational Mesh

Flow and Boundary conditions

Two dimensionless parameters, Reynolds number (*Re*) and Froude number (*Fr*) respectively, are defined as:

$$Re = \frac{UD}{\nu} \tag{6}$$

$$Fr = \frac{U}{\sqrt{gD}} \tag{7}$$

where U is the flow velocity, ν is the kinematic viscosity of water and g is the gravitational acceleration. Here, the case at Re=27000 and Fr=0.8 is chosen. Because the relatively high Froude number can show more significant differences caused by the free surface.

A uniform flow is set at the velocity inlet and zero-Gradient boundary condition is applied to the pressure outlet. A no-slip boundary condition is imposed to the cylinder surface. Besides, the symmetry boundary condition is used for the bottom. But unlike the single-phase flow, zero-Gradient boundary conditions are adopted for the sides rather than the symmetry boundary condition. Because the wake flow spreads quickly along the width especially near the interface.

The non-dimensional time-step $\Delta tU/D$ is set to 0.002 to ensure the maximum courant number is below 0.5. The duration of simulation for the data analysis is between non-dimensional time $tU/D=100$ and $tU/D=200$ when the lift force has been periodic stabilized. All simulations are conducted on the high performance computing (HPC) platform of CMHL at Shanghai Jiao Tong University. The processors of each node are 2×Intel Xeon Gold 5120 (14 Cores, 2.20Ghz) with 128 GB memory and two nodes are used for each case. For the medium mesh case, the CPU time for the specified time interval ($tU/D=100$ - $tU/D=200$) is about 160 h.

RESULTS AND DISCUSSION

Surface elevation

For two-phase flow, it is essential to capture the interface accurately. And the surface elevation is often used to evaluate it as an important parameter. In the present study, RANS method can only give time-averaged solutions while the fluctuations of the flow will not reflected in the results evidently. So, this section will only focus on the comparison of the mean surface elevation although more information such as rms value are provided by experiment.

Fig. 3 shows the profiles of the mean surface elevation at two transverse planes. It is shown the results agree well with the experimental data and LES results in general. The current method can capture the surface well especially in the near filed where is the most concerned region. The mesh density does not influence the results significantly and the only difference may occur in area away from the center line, as shown in Fig. 3(a). Considering the accuracy and cost, the medium mesh is chosen for the following analysis.

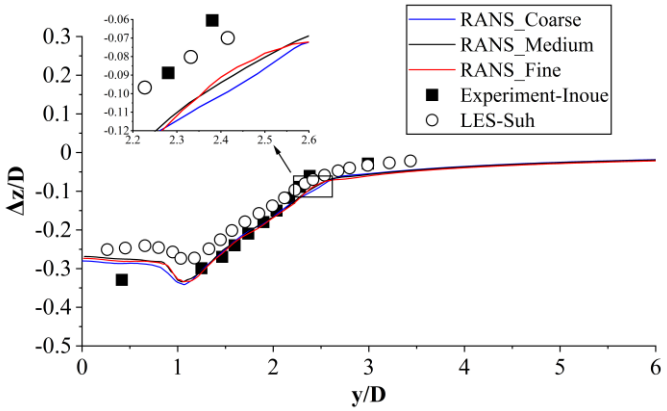

(a) x=0.9D

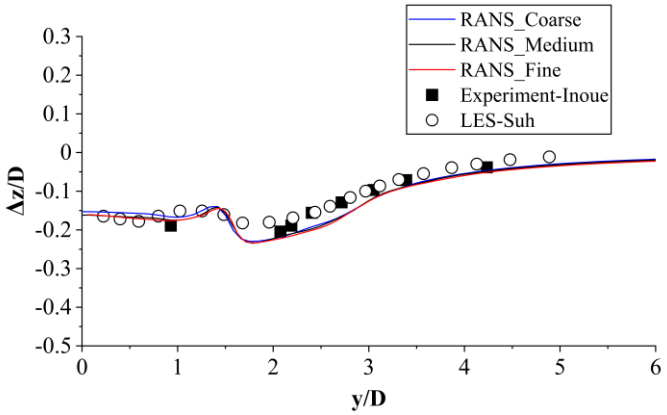

(b) x=2D
Fig 3. Profiles of the mean surface elevation

Fig. 4 shows the contour lines of the mean surface elevation compared with the experiment. The overall distribution is considered to be in good agreement with the results of experiment including the regions of depression and the locations of the waves. But the bow wave in front of the cylinder seems more steeper in the experiment than present simulation.

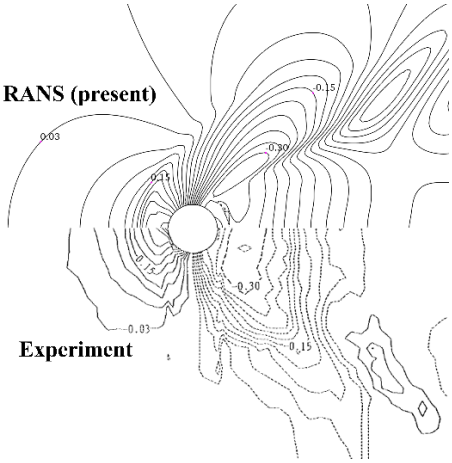

Fig 4. Contour lines of the mean surface elevation

Fig. 5 illustrates the mean wave run-up height and depression depth. The distance from the maximum surface elevation to the still water is defined as the wave run-up height and the minimum surface elevation corresponds to the depression depth. It can be seen the normalized mean run-up height is 0.339 and the depression depth is 0.310.

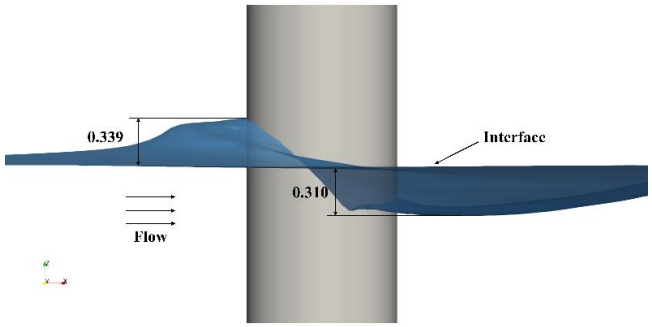

Fig 5. Mean wave run-up height and depression depth

Profiles of the mean surface elevation on the cylinder surface are plotted in Fig. 6. The minimum surface elevation on the cylinder surface occurs at approximately 110°. The discrepancy in the rear part of the cylinder implies that the depression region may be sensitive to the mesh density.

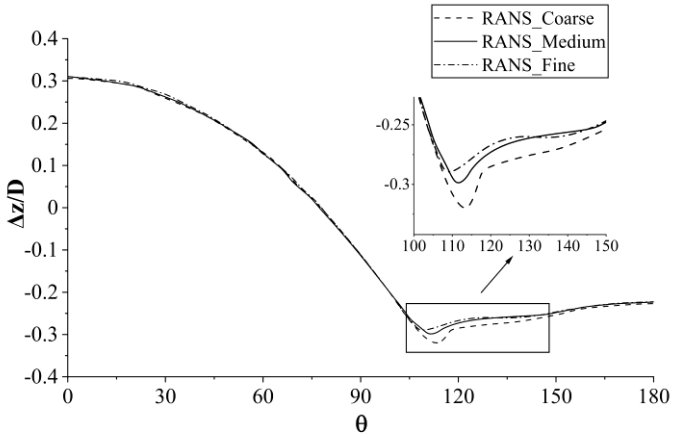

Fig 6. Profiles mean surface elevation on the cylinder surface

Fig. 7 shows the iso-surface of alpha.waterMean=0.5 which represents the interface between air and water. It can be clearly observed that bow wave appears in front of the cylinder and depression is formed behind the cylinder. Besides, Kelvin waves can be seen in the far field.

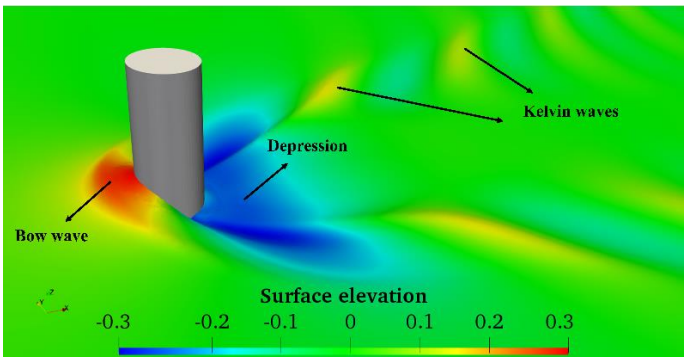

Fig 7. Iso-surface of alpha.waterMean=0.5

Hydrodynamic forces

The drag and lift coefficients are defined as follows:

$$C_D = \frac{F_{Drag}}{\frac{1}{2}\rho U^2 DL} \tag{8}$$

$$C_L = \frac{F_{lift}}{\frac{1}{2}\rho U^2 DL} \tag{9}$$

Here, L is taken as the immersed length in the still water and ρ is the density of the water. The results of $\overline{C_D}$ and C_L^{rms} are listed in Table 1. The data required for the calculation is selected from $tU/D = 100$ and $tU/D = 200$ which the flow is considered to be stable.

It is obvious that the present results agree well with the LES results in terms of the mean drag coefficients. However, the root-mean-square (rms) value of the lift coefficient is under-predicted by current method. The reason for it is necessary to be further analyzed. In addition, the medium mesh is capable of predicting hydrodynamic forces in this case.

According to the Reynolds number, this case is in the sub-critical regime which are defined for turbulent flow past the circular cylinder. For single-phase flow, many experiments and numerical simulations have demonstrated that the mean drag coefficient is approximately a constant of 1.2 in this regime. Compared with it, the existence of free surface brings a significant reduction of it which can reach about 16.7% in this case.

Table1. Hydrodynamic force coefficients on cylinder

Mesh	$\overline{C_D}$	C_L^{rms}
Coarse	0.950	0.102
Medium	0.956	0.100
Fine	0.951	0.097
LES by Suh et al.	0.984	0.220
LES by Kawamura et al.	0.970	0.240

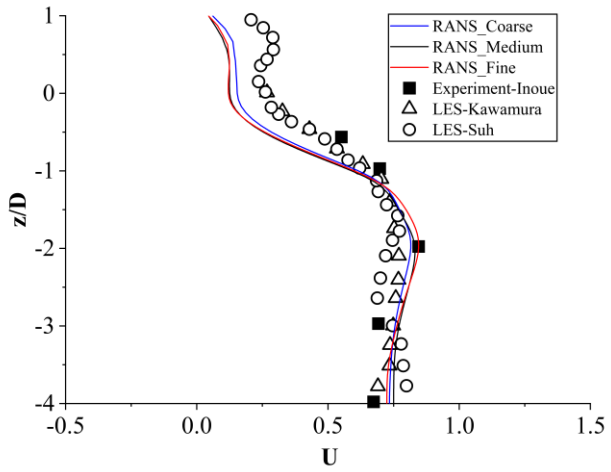

Fig 8. Profiles of the mean streamwise velocity at x=4.5D and y=0

Wake field characteristics

Profiles of the mean streamwise velocity behind the cylinder at x=4.5D is presented in Fig. 8. The results at lower part agree well with the experimental data and LES results. However, the present simulation under-predict the velocity from z/D=-1 to interface. It shows the streamwise velocity recovers slower than expected and the length of recirculation seems to be longer using current method. In addition, the results are not greatly affected by the mesh density as shown in Fig. 8 and it confirms the conclusion mentioned above.

Fig. 9 shows the profiles of the mean streamwise velocity at x=1.06D. At the interface, it can be seen the width of the wake is wider and the streamwise velocity recovers slower compared with the other depth. Profiles of the mean transverse velocity at x=1.06D are compared in Fig. 10. The significant outward transverse velocity can be observed at the interface and the same but weaker phenomenon can still be found at z=-0.5D. Below the plane of z=-0.5D, the transverse velocity points toward the central line of the cylinder again in the deep region. And it may explain why the wake is spread along the width quickly near the interface.

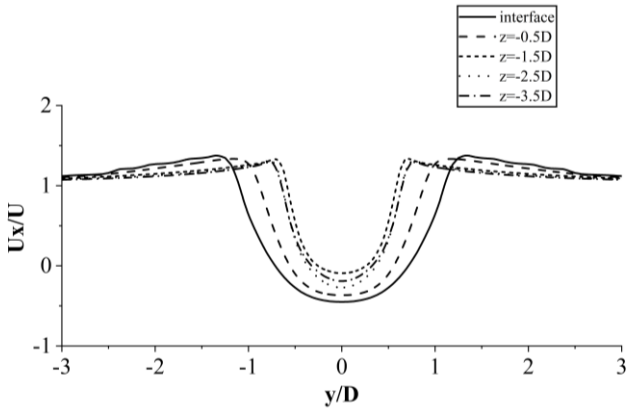

Fig 9. Profiles of the mean streamwise velocity at x=1.06D

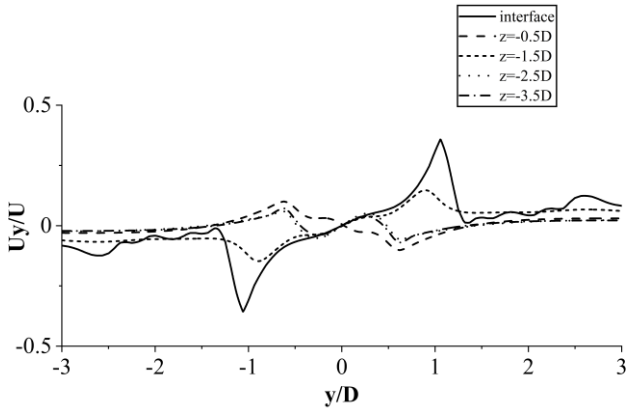

Fig 10. Profiles of the mean transverse velocity at x=1.06D

For a better understanding of the complicated flow near the interface, streamlines are visualized in Fig. 11. At the interface, two large vortical eddies can be observed in the depression region which are defined as the recirculation bubble (Kirkil et al., 2015). Due to the existence of free surface, the width and length of it are larger than the ones in deep region where the flow pattern is more similar to single-phase flow. Fig. 11(b) shows the streamlines of the plane at y=0 and it can reveal the changes of the flow in the vertical direction. It can be seen the flow is strongly disturbed by two vortices near the interface. However, few vertical changes can be found in the deep flow. Moreover, the separation line is well represented on the cylinder surface which will be discussed later.

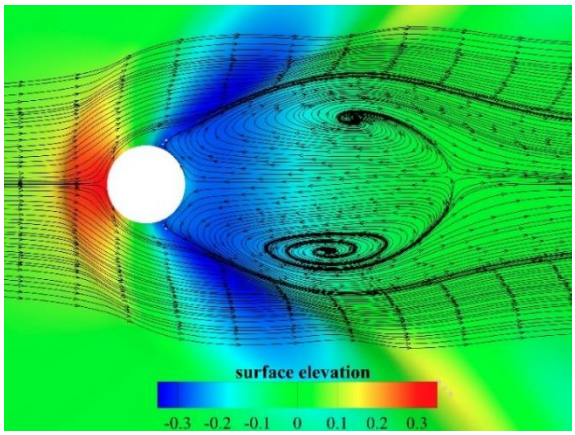

(a) Interface

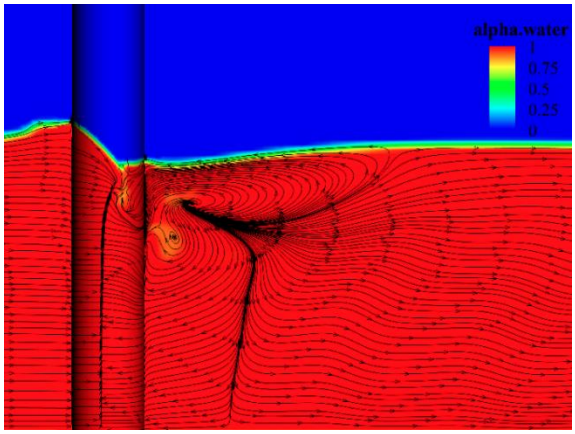

(b) slice of the vertical plane at y=0

Fig 11. Instantaneous streamlines at interface and vertical plane(y=0)

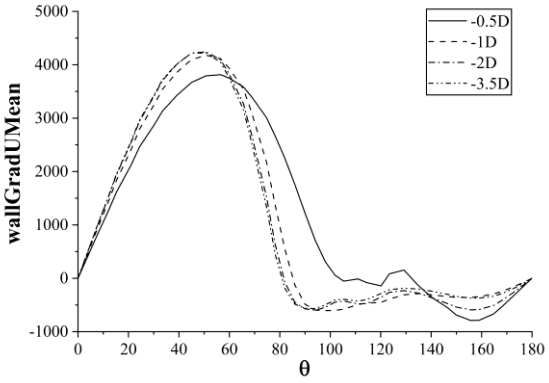

Fig 12. Mean velocity gradient on the cylinder surface

The separation angle can be determined by the plot of velocity gradient on the cylinder surface which is shown as Fig. 12. When the point satisfies $du/dn = 0$, it represents the location of separation point. As the depth increases, the separation angle gradually decreases and tends to remain the same in the deep flow. It can also be confirmed qualitatively in Fig. 11(b). This trend is consistent with the LES results by Suh (2011). It shows the existence of free surface delays the transition in the shear layer and the effect can be almost negligible in the region

z<-2D. Fig. 13 shows the mean pressure coefficient on the cylinder surface. The adverse pressure gradient is reduced near the interface and it may explain why the separation point moves backward.

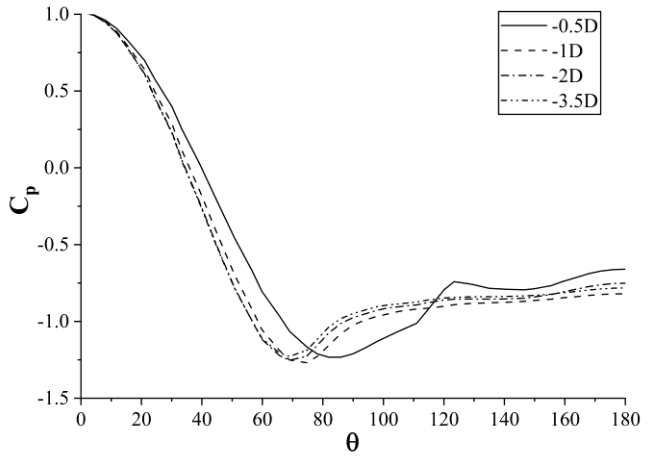

Fig 13. Mean pressure coefficient on the cylinder surface

As is known, vortex shedding is one of the most important features in such problems. Fig. 14 visualizes the distribution of the instantaneous vertical vorticity at several depths to explore the development of it. At the interface, two separated shear layers are deviated from the center line. Hence, the interaction between layers is weak and no vortex shedding is formed in the wake obviously. At z=-0.5D, the flow pattern is similar to that at the interface. It can be clearly seen that the layers are still inclined outward although the separation point moves backward. However, regular vortex shedding can be observed in the region below the plane of z/D=-2, which indicates the vortex shedding is attenuated near the interface.

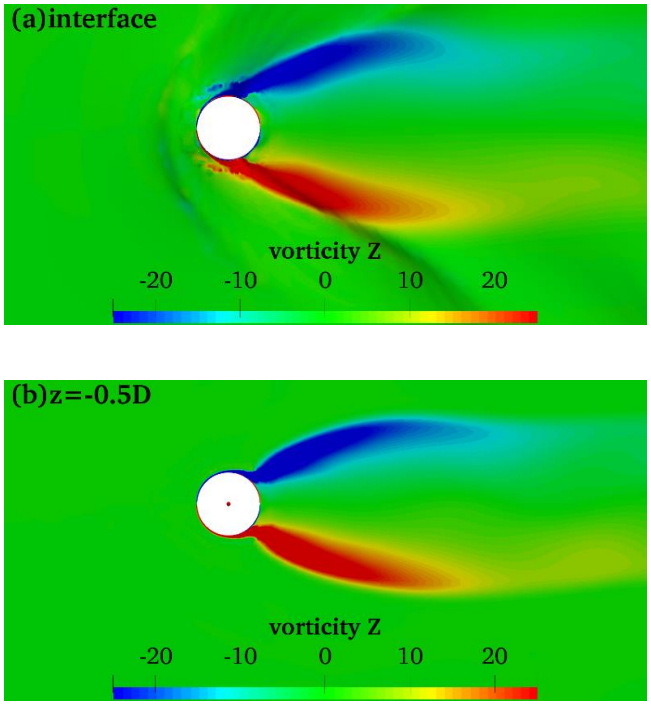

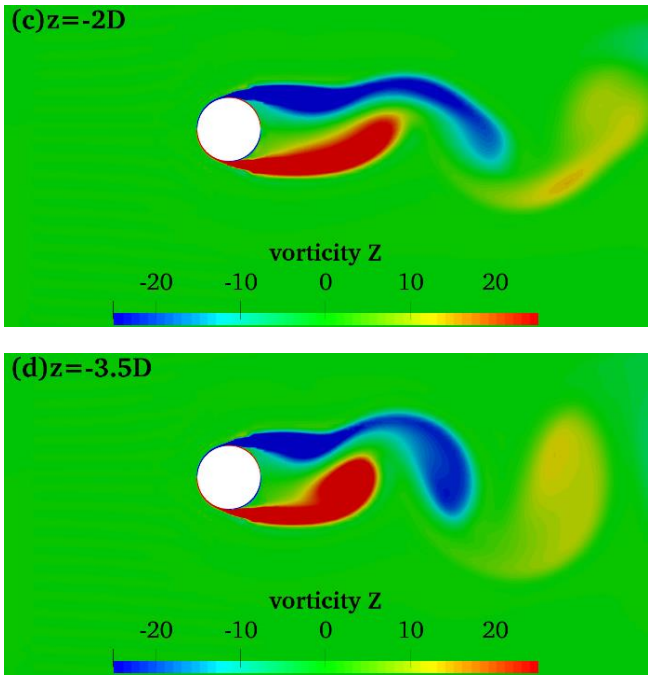

Fig 14. Instantaneous vertical vorticity at interface and horizontal planes

Fig. 15 shows the iso-surface using the Rortex method (Liu et al., 2015; Liu et al., 2018) which represents the vortical structures. This method defines a new vector to describe the rotation and can clearly shows the vortical structures especially for the weak vortices. With this method, it is found that the regular vortex shedding is attenuated near the interface. But some weak vortices still can be observed in the far field. Besides, the necklace vortices appear in front of the cylinder as described by Suh (2011).

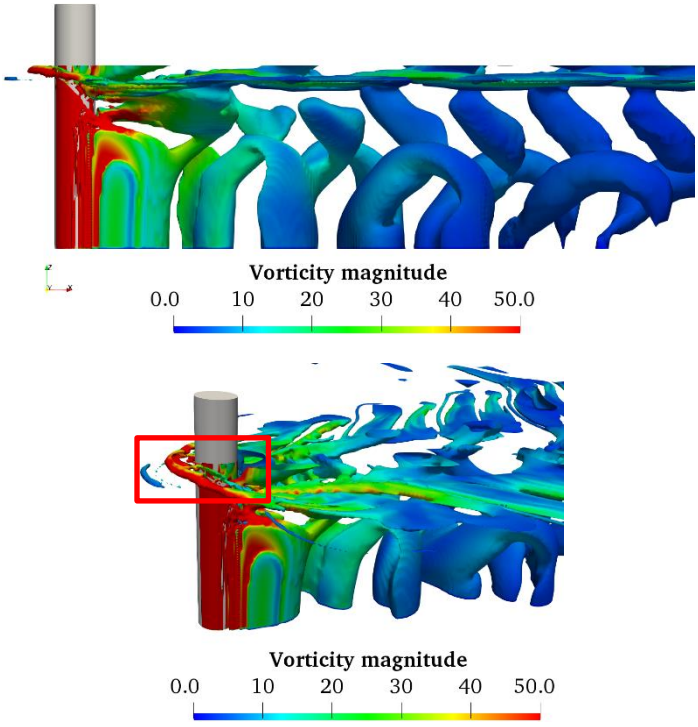

Fig 15. Instantaneous vortical structures (Rortex method)

CONCLUSIONS

In the present work, the effect of free surface on flow around a surface piercing cylinder is investigated by the CFD approach. The in-house CFD solver naoe-FOAM-SJTU is used to simulate the flow, which solves the RANS equations and incorporates the VOF method. The comparison with experiment and LES simulations is conducted to verify the reliability of the current method. Based on the detailed analysis of the results, the conclusions are as follows:

(1) The mean surface elevation is in good agreement with the experiment and previous LES simulations. The overall distribution including the depression region and wave peaks is basically same with the experiment. And the bow wave, depression and Kelvin waves can be observed at the interface.

(2) For hydrodynamic forces, the comparison with the single-phase flow shows that the existence of free surface brings a reduction in terms of the drag coefficient which can reach 16.7% in this case.

(3) The profiles of the mean velocity in the wake especially at the interface is rather different. The size of the recirculation bubble at the interface becomes larger because of the interaction between air and water. And the disturbance is found near the interface in the vertical direction. The transition in the shear layers is delayed by the free surface, which is indicated by the separation angle. The vortex shedding is attenuated near the interface and can only be observed in the deep flow.

The above study proves that the current method is reliable and can capture the time-averaged characteristics in this case. Nevertheless, more detailed information like smaller vortices and fluctuation of the flow field can not be given limited by RANS method. So, it is necessary to apply DES or LES method to improve the accuracy in the future work.

ACKNOWLEDGEMENTS

This work is supported by the National Natural Science Foundation of China (51879159), The National Key Research and Development Program of China (2019YFB1704200, 2019YFC0312400), Chang Jiang Scholars Program (T2014099), and Innovative Special Project of Numerical Tank of Ministry of Industry and Information Technology of China (2016-23/09), to which the authors are most grateful.

REFERENCES

Chaplin, JR, and Teigen, P (2003). "Steady flow past a vertical surface-piercing circular cylinder," *Journal of Fluids and Structures*, 18(3-4), 271-285.

Inoue, M, Bara, N, and Himeno, Y (1993). "Experimental and numerical study of viscous flow field around an advancing vertical circular cylinder piercing a free-surface," *Journal of the Kansai Society of Naval Architects*, 220, 57–64.

Kawamura, T, Mayer, S, Garapon, A, and Sørensen, L (2002). "Large Eddy Simulation of a Flow Past a Free Surface Piercing Circular Cylinder," *Journal of Fluids Engineering*, 124(1), 91-101.

Kirkil, G, and Constantinescu, G (2015). "Effects of cylinder Reynolds number on the turbulent horseshoe vortex system and near wake of a surface-mounted circular cylinder," *Physics of Fluids*, 27(7), 075102.

Koo, BG (2011). "Numerical study of two-phase air-water interfacial flow: plunging wave breaking and vortex-interface interaction," PhD Thesis, University of Iowa, USA.

Liu, C, Gao, Y, Tian, S, and Dong, X (2018). "Rortex a new vortex vector definition and vorticity tensor and vector decompositions," *Physics of Fluids*, 30(3), 035103.

Liu, J, and Liu, C (2019). "Modified normalized Rortex/vortex identification method," *Physics of Fluids*, 31(6), 061704.

Pereira, FS, Vaz, G, and Eça, L (2019). "Evaluation of RANS and SRS methods for simulation of the flow around a circular cylinder in the sub-critical regime," *Ocean Engineering*, 186, 106067.

Suh, J, Yang, J, and Stern, F (2011). "The effect of air–water interface on the vortex shedding from a vertical circular cylinder," *Journal of Fluids and Structures*, 27(1), 1-22.

Wang, JH, Zhao, WW, and Wan, DC (2019). "Development of naoe-FOAM-SJTU solver based on OpenFOAM for marine hydrodynamics," *Journal of Hydrodynamics*, 31, 1–20.

Williamson, CHK (2003). "Vortex dynamics in the cylinder wake," *Annual Review of Fluid Mechanics*, 28(1), 477-539.

Ye, H, and Wan, DC (2017). "Benchmark computations for flows around a stationary cylinder with high Reynolds numbers by RANS-overset grid approach," *Applied Ocean Research*, 65, 315-326.

Yeon, SM, Yang, J, and Stern, F (2016). "Large-eddy simulation of the flow past a circular cylinder at sub- to super-critical Reynolds numbers," *Applied Ocean Research*, 59, 663-675.

Yu, G, Avital, EJ, and Williams, JJR (2008). "Large Eddy Simulation of Flow Past Free Surface Piercing Circular Cylinders," *Journal of Fluids Engineering*, 130(10), 101304.

Zhang, D (2017). "Comparison of Various Turbulence Models for Unsteady Flow around a Finite Circular Cylinder at Re=20000", *Journal of Physics: Conference Series*, 910, 012027.

Zhao, WW, Wan, DC, and Sun, R (2016). "Detached-Eddy Simulation of Flows over a Circular Cylinder at High Reynolds Number," *Proceedings of the Twenty-sixth International Ocean and Polar Engineering Conference*, Rhodes, Greece, 1074-1079.

Zhao, WW, Wang, JH, and Wan, DC (2020). "Vortex identification methods in marine hydrodynamics," *Journal of Hydrodynamics*, 32, 286-295.